



# Unsteady Boundary Layer Flow over a Vertical Surface due to Impulsive and Buoyancy in the Presence of Thermal-Diffusion and Diffusion-Thermo using Bivariate Spectral Relaxation Method

S. S. Motsa<sup>1</sup> and I. L. Animasaun<sup>2†</sup>

<sup>1</sup> *School of Mathematics, Statistics & Computer Science, University of KwaZulu-Natal, Private Bag X01, Scottsville, Pietermaritzburg, 3209, South Africa.*

<sup>2</sup> *Department of Mathematical Sciences, Federal University of Technology, Akure, Ondo State Nigeria.*

† *Corresponding Author Email: anizakph2007@gmail.com*

(Received September 12, 2015; accepted November 8, 2015)

## ABSTRACT

In this article, unsteady boundary layer flow formed over a vertical surface due to impulsive motion and buoyancy is investigated. The mathematical model which properly accounts for space and temperature-dependent internal heat source in a flowing fluid is incorporated into the energy equation. This model is presented in this study as a term which accounts for two different forms of internal heat generation during the short time period and long time period. Due to the fluid flow under consideration, the influence of thermal-diffusion and diffusion-thermo are incorporated into the governing equation since it may not be realistic to assume that both effects are of smaller order of magnitude than the effects described by Fourier's or Fick's law. The corresponding effect of internal heat source on viscosity is considered; the viscosity is assumed to vary as a linear function of temperature. The flow model is described in terms of a highly coupled and nonlinear system of partial differential equations. The governing equations are non-dimensionalized by using suitable similarity transformation which unraveled the behavior of the fluid flow at short time and long time periods. The dimensionless system of non-linear coupled partial differential equations (PDEs) is solved using Bivariate Spectral Relaxation Method (BSRM). A parametric study of selected parameters is conducted and results of the surface shear stress, heat transfer and mass transfer at the wall are illustrated graphically and physical aspects of the problem are discussed.

**Keywords:** Unsteady; Mixed convection; Impulsive motion; Variable viscosity; Bivariate Spectral Relaxation method; Space-heat source.

## NOMENCLATURE

$a$	stretching rate	$T_m$	mean fluid temperature
$A^*$	space dependent internal heat source	$u$	fluid velocity along $x$ -direction
$B^*$	temperature dependent internal heat source	$u_e$	stretching velocity at freestream
$C$	concentration of the fluid	$v$	fluid velocity along $y$ -direction
$C_f$	skin friction coefficient	$\beta$	volumetric coefficient of thermal expansion
$C_p$	specific heat at constant pressure	$\beta^*$	volumetric coefficient of concentration expansion
$C_s$	concentration susceptibility	$\eta$	similarity variable (space)
$D_m$	coefficient of mass diffusivity	$\theta(\eta, \xi)$	dimensionless temperature function
$f'(\eta, \xi)$	dimensionless velocity function	$\vartheta$	kinematic viscosity
$g$	acceleration due to gravity	$\kappa$	thermal conductivity of the fluid
$N_u$	Nusselt number	$\mu$	viscosity of the fluid
$Re_x$	Reynold number	$\xi$	dimensionless time scale
$Sh$	Sherwood number		
$t$	dimensional time		
$T$	temperature of the fluid		

$\rho$	density of the fluid	$\omega$	dimensionless variable viscosity parameter
$\tau$	dimensional time	$T_w, C_w$	condition of $T, C$ at the vertical wall
$\phi(\eta, \xi)$	dimensionless concentration function	$T_\infty, C_\infty$	condition of $T, C$ at freestream
$\Psi(x, y)$	stream function		

### 1. INTRODUCTION

The study of the thin layer formed on either horizontal or vertical surface as fluid flows over it has received great attention because of its applications in industry and engineering processes. According to thermopedia, mixed convection is a combination of forced and free convection which is the general case of convection when a flow is determined simultaneously by both an outer forcing system (i.e., outer energy supply to the fluid streamlined body system) and inner volumetric (mass) forces by the nonuniform density distribution of fluid medium in a gravity field; Petukhov and Poliakov (1988). Mass transfer occurs in many processes with extensive applications in chemical engineering such as reaction engineering, separations engineering, heat transfer engineering and many other sub-disciplines of chemical engineering Welty *et al.* (1976). Mass transfer is used by different scientific disciplines mostly for modeling physical processes and mechanisms that involve diffusive and convective transport of chemical species within physical systems Bird *et al.* (2007). In many industrial manufacturing processes, external support might be required to enhance the flow along a vertical surface; such fluid flow may also be induced by an impulsively (i.e. time-dependent) stretching of the fluid layer adjacent to surface or fluid layers at the free stream. Recently, Animasaun (2015a) reported the uses of modified Boussinesq approximation to investigate double diffusive convective micropolar flow over a surface in which  $T_w < T_\infty$ . Effects of non-uniform dual temperature-dependent heat generation/absorption on a stagnation-point flow of Jeffrey nanofluid is presented in Sandeep *et al.* (2016).

Theoretically and practically, Fourier's law of heat conduction describes the relation between energy flux and temperature gradient. Fick's law was determined by the correlation of mass flux and concentration gradient; see Fick (1855). Fourier (1995) reported that energy flux can be generated by composition gradients, pressure gradients or body forces. The energy flux caused by composition gradient was discovered in 1873 by G. Henri Dufour and was correspondingly referred to as Dufour effect; on the other hand, mass flux can also be cre-

ated by a temperature gradient, as it was established by Charles Soret. Practically speaking, energy flux due to mass (concentration) gradient tends to occur as a coupled effect of irreversible processes in the industry when impulsive and buoyancy are required to induce the flow. For example, when species are introduced at a surface in fluid domain with different (lower) density than the surrounding fluid, both Soret (thermo-diffusion) and Dufour (diffusothermal) effects tends to be influential. This is often encountered in chemical engineering processes according to Fourier (1995), Fick (1855) and Alam *et al.* (2006). It is worth mentioning that when Dufour effect together with its reciprocal phenomenon (Soret effect) are considered in most studies on heat and mass transfer; the non-linearity of the governing partial differential equation which denotes the mathematical modeling increases and becomes more difficult to solve. In view of this, an efficient numerical method/technique is required to solve and investigate the behavior of this kind of fluid flow. To solve a related mathematical problem, Rashad *et al.* (2015) adopted implicit iterative finite-difference scheme to solve dimensionless governing equations which involve second derivative of temperature in species (mass) equation and second derivative of concentration in the energy equation.

On December 9, 1850 the word "impulsive" was used to describe fluid flow by Sir George Stokes; for details, see the 47th point in Stoke (1901). Thereafter, series of investigations have been carried out towards the understanding of the dynamics of impulsive induced fluid flow. The motion within the boundary layer that arises when a semi-infinite flat plate is impulsively started from rest with velocity  $U$  was investigated by Stewartson (1951). The boundary layer flow development of a viscous fluid on a semi-infinite flat plate due to impulsive motion of the free stream has been further investigated in Dennis (1972) and Watkins (1975). Williams and Rhyne (1980) argued extensively that the viscous flow within the boundary layer develops slowly, reaching a fully develop steady flow only after some period of time. The boundary layer development occurs in two stages (at a small time and at a large time). Upon using the scaling developed in Williams and Rhyne (1980), it seems difficult to obtain analytic so-

lutions of unsteady boundary layer flows valid for all time. To obtain solutions of unsteady boundary layer flows which are valid for all time Nath *et al.* (2002) examined the asymptotic behavior of the solution for a steady case and later obtained the solution for both cases (unsteady and steady) by using an implicit finite difference scheme. Sandeep and Sugunamma (2014) adopted Laplace transform technique to solve the reduced dimensionless equations which modeled unsteady hydro-magnetic free convection and radiative heat transfer along a vertical surface due to impulsive. It is worth mentioning that the uses of Laplace transform strongly depend on the non-linearity of the differential equation. A perturbation technique which only provides a valid solution for small time was adopted in Dennis (1972). To obtain this kind of solution over the domain corresponding to the dimensionless time ( $0 \leq \xi \leq 1$ ), Pop *et al.* (2004) adopted Keller-box implicit finite difference method to obtain the numerical solution. Liao (2006) explained the limitations of the numerical approach adopted in Nath *et al.* (2002) and Nazar *et al.* (2004) and hence presented analytic solutions uniformly valid for all dimensionless time ( $0 \leq \xi < +\infty$ ) in the whole space region ( $0 \leq \eta < +\infty$ ) using Homotopy analysis method (HAM).

Spectral Methods are the class of spatial discretization of differential equations. They provide a way of translating an equation expressed in continuous space and time into a discrete equation which can be solved numerically. Spectral discretizations of differential equations are based on Fourier or Chebyshev series which provides a very low error approximations Canuto *et al.* (1988). Considering the fact that spectral methods are computationally less expensive, Spectral Homotopy Analysis method of solving boundary value problems was proposed in Sibanda *et al.* (2010). Motsa (2013b) modified spectral homotopy analysis method (SHAM) and successfully used Local Linearisation Method (LLM) to solve a partial differential equation (PDE) which models the problem of unsteady boundary layer flow caused by an impulsively stretching plate. The idea of decoupling systems of equations that were called local linearisation method (LLM) in Motsa (2013a) have been extended to a new spectral collocation method (BSLLM) which have been implemented to solve the problem of unsteady heat and mass transfer past a semi-infinite vertical plate with diffusion-thermo and thermophoresis effects in the presence of suction; see Motsa and Animasaun (2015). Just of recent, Motsa

*et al.* (2015) presented the ideas of Gauss-Seidel approach to decoupling nonlinear system of PDEs into a sequence of linear partial differential equations which are then solved using the Chebyshev spectral collocation method with bivariate Lagrange interpolation polynomials as basis functions. The method called Bivariate Spectral Relaxation Method (BSRM) involves seeking for solutions that are expressed as bivariate Lagrange interpolating polynomials and applying pseudospectral collocation in both independent variables of the governing PDEs.

In all the above studies little or no attention has been given to investigate unsteady boundary layer flow over a vertical surface due to impulsive motion and buoyancy in the presence of thermal-diffusion and diffusion-thermo. In this study space and temperature-dependent internal heat source is adopted and its corresponding influence on the fluid viscosity is investigated. The Bivariate Spectral Relaxation Method is adopted to obtain the numerical solutions of the systems of highly non-linear partial differential equations. It is worth mentioning that the results of this present study will provide useful information to engineers in the industry and most especially to chemical engineers. In this article, we present the mathematical formulation of the problem in section 2. The numerical solution of the dimensionless equations using Bivariate Spectral Relaxation method is presented in section 3. In section 4 the results and discussions are explained and we present the conclusions based on the findings in section 5.

## 2. GOVERNING EQUATIONS

Consider the flow of a viscous incompressible fluid past a vertical plate with the effects thermal diffusion, diffusion-thermo and viscous dissipation heat in the presence of exponential decaying heat source. In this research, a case where the fluid is emerging out of a slit at the origin ( $x = 0, y = 0$ ) and moving along the vertical wall is considered. As shown in Fig. 1.,  $x$ -axis is taken along the plate in the vertically upward direction and  $y$ -axis is normal to the vertical surface.

Initially, at  $t \leq 0$  the plate and the adjacent fluid is of low temperature ( $T_\infty$ ) and low concentration ( $C_\infty$ ) in a stationary condition. At  $t > 0$  the inviscid flow is given an impulsive motion in the vertical direction against the gravitational field with velocity  $u_e = ax$  and both the temperature and concentration level near the plate are raised from  $T_\infty$  to  $T_w$  and  $C_\infty$  to  $C_w$  respectively. This is based on the fact that  $T_\infty < T_w$  and  $C_\infty < C_w$ . The surface of the plate is as-

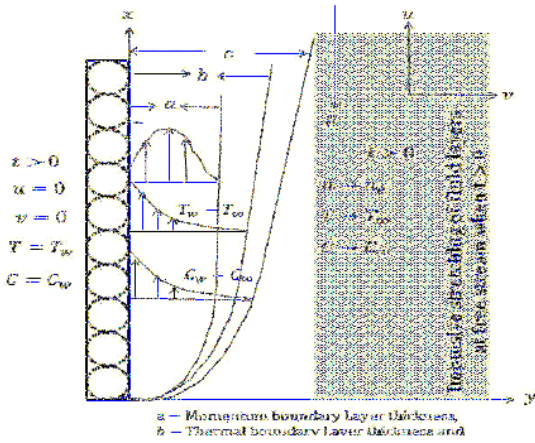


**Fig. 1. Physical Model and coordinate.**

sumed to have an arbitrary constant temperature  $T_w$ . In this investigation, the unsteadiness in the flow field is caused by impulsively induced motion in the free stream (i. e. the unsteadiness is caused by a change in the free stream velocity with respect to time) and by a sudden increase in temperature and concentration at the surface. The density variation and the buoyancy effects are taken into consideration so that the Boussinesq approximation for both the temperature and concentration gradient is adopted. Under these assumptions along with boundary layer approximations, the flow is governed by the following system of equations

$$\frac{\partial u}{\partial x} + \frac{\partial v}{\partial y} = 0, \tag{1}$$

$$\frac{\partial u}{\partial t} + u \frac{\partial u}{\partial x} + v \frac{\partial u}{\partial y} = u_e \frac{\partial u_e}{\partial x} + \frac{1}{\rho} \frac{\partial}{\partial y} \left( \mu \frac{\partial u}{\partial y} \right) + g\beta(T - T_\infty) + g\beta^*(C - C_\infty), \tag{2}$$

$$\frac{\partial T}{\partial t} + u \frac{\partial T}{\partial x} + v \frac{\partial T}{\partial y} = \frac{\kappa}{\rho C_p} \frac{\partial^2 T}{\partial y^2} + \frac{D_m K_t}{C_p C_s} \frac{\partial^2 C}{\partial y^2} + \left( \frac{1}{1 - e^{-\tau}} \right) \times$$

$$\frac{\kappa a}{\rho C_p \vartheta} \left[ A^*(T_w - T_\infty) e^{\left( -y \sqrt{\frac{a}{\vartheta \xi}} \right)} + B^*(T - T_\infty) \right], \tag{3}$$

$$\frac{\partial C}{\partial t} + u \frac{\partial C}{\partial x} + v \frac{\partial C}{\partial y} = D_m \frac{\partial^2 C}{\partial y^2} + \frac{D_m K_t}{T_m} \frac{\partial^2 T}{\partial y^2}. \tag{4}$$

The initial conditions are given at  $t \leq 0$  as

$$u = 0, \quad v = 0, \quad T = T_\infty, \quad C = C_\infty. \tag{5}$$

The boundary conditions for  $t > 0$  are

$$u = 0, \quad v = 0, \quad T = T_w, \quad C = C_w \quad \text{at } y = 0, \tag{6}$$

$$u \rightarrow u_e, \quad T \rightarrow T_\infty, \quad C \rightarrow C_\infty \quad \text{as } y \rightarrow \infty. \tag{7}$$

Since heat and mass transfer occur simultaneously in the moving fluid due to impulsive and buoyancy, the relations between the fluxes and the driving potentials are of more intricate in nature. In view of these effects, thermal-diffusion and the diffusion-thermo terms were incorporated into Eq. (3) and Eq. (4). Internal energy generation can be explained as a scientific method of generating heat energy within a body by a chemical, electrical or nuclear process. Natural convection induced by internal heat generation is a common phenomenon in nature. In many situations, there may be an appreciable temperature difference between the surface and the ambient fluid. This necessitates the consideration of temperature dependent heat sources that may exert a strong influence on the heat transfer characteristics Salem and El-Aziz (2007). El-Aziz and Salem (2008) further stated that exact modeling of internal heat generation or absorption is quite difficult and argued that some simple mathematical models can express its average behavior for most physical situations. This idea is used to model the space and temperature dependent heat source in Eq. (2) such that its influence on the heat and mass transfer at a short time and long time periods exist. In this study, the fluid viscosity ( $\mu$ ) is assumed to vary as a linear function of temperature. This assumption is valid based on the fact that the internal heat source will increase the amount of total temperature of the fluid as it flows over a vertical surface. Following Mukhopadhyay (2009), the mathematical model of temperature-dependent viscosity model which was developed using the experimental data of Batchelor (1987) as

$$\mu(T) = \mu^* [m_1 + b(T_w - T)], \tag{8}$$

is considered. This consideration is based on the discussion in Animasaun (2015b) on the physical effect of time-dependent modified thermal Grashof number and time-dependent modified solutal Grashof number on the behavior of fluid flow along a vertical surface. The following relations are introduced to transform  $u$ ,  $v$ ,  $T$  and  $C$  as

$$u = \frac{\partial \psi}{\partial y}, \quad v = -\frac{\partial \psi}{\partial x}, \quad \theta = \frac{T - T_\infty}{T_w - T_\infty}, \quad \phi = \frac{C - C_\infty}{C_w - C_\infty}. \tag{9}$$

respectively. Here,  $\psi(x, y)$  is the stream function. In formulating the problem of the boundary layer development which is impulsively set into motion, one encounters the problem of determining the appropriate scaling for the problem. The solution for small dimensionless time ( $\tau$ ) is similar in the scaled coordinate  $\frac{y}{\sqrt{\vartheta t}}$  (i.e. the solution exists for small time) while the solution for large time is similar in the scaled coordinate  $y\sqrt{\frac{u_e}{\vartheta x}}$  (i.e. the solution exists for large time). This implies that we have to find a scaling of the  $y$ -coordinate which behaves like  $\frac{y}{\sqrt{\vartheta t}}$  for small time and as  $y\sqrt{\frac{u_e}{\vartheta x}}$  for large time. Furthermore, it is convenient to choose a time scale  $\xi$  so that the region of time integration may become finite. Following Williams and Rhyne (1980), such similarity transformations are

$$\eta = y\sqrt{\frac{a}{\vartheta \xi}}, \quad \frac{\psi(x, y)}{x\sqrt{a\vartheta \xi}} = f(\eta, \xi), \quad \xi = 1 - e^{-\tau}, \quad \tau = at. \tag{10}$$

Substituting Eq. (8) - Eq. (10) into Eq. (1) - Eq. (7), Eq. (1) is identically satisfied and Eq. (2) - Eq. (7) reduces to

$$[m_1 + \omega - \theta\omega] \frac{\partial^3 f}{\partial \eta^3} - \omega \frac{\partial \theta}{\partial \eta} \frac{\partial^2 f}{\partial \eta^2} + \frac{\eta}{2}(1 - \xi) \frac{\partial^2 f}{\partial \eta^2} + \omega G_r \theta +$$

$$\xi \left[ 1 + f \frac{\partial^2 f}{\partial \eta^2} - \left( \frac{\partial f}{\partial \eta} \right)^2 \right] + \omega G_s \phi = \xi(1 - \xi) \frac{\partial^2 f}{\partial \xi \partial \eta}, \tag{11}$$

$$\frac{\partial^2 \theta}{\partial \eta^2} + \frac{\eta}{2} Pr(1 - \xi) \frac{\partial \theta}{\partial \eta} + Pr \xi f \frac{\partial \theta}{\partial \eta} + \frac{\{A^* e^{-\eta} + B^* \theta\}}{[m_1 + \omega - \theta\omega]}$$

$$+ Pr D_f \frac{\partial^2 \phi}{\partial \eta^2} = \xi(1 - \xi) Pr \frac{\partial \theta}{\partial \xi}, \tag{12}$$

$$\frac{\partial^2 \phi}{\partial \eta^2} + \frac{\eta}{2} Sc(1 - \xi) \frac{\partial \phi}{\partial \eta} + Sc \xi f \frac{\partial \phi}{\partial \eta} + Sc Sr \frac{\partial^2 \theta}{\partial \eta^2} =$$

$$\xi(1 - \xi) Sc \frac{\partial \phi}{\partial \xi}. \tag{13}$$

The boundary conditions reduces to

$$f(0, \xi) = \frac{\partial f(0, \xi)}{\partial \eta} = 0, \quad \theta(0, \xi) = \phi(0, \xi) = 1, \tag{14}$$

$$\frac{\partial f(\infty, \xi)}{\partial \eta} \rightarrow 1, \quad \theta(\infty, \xi) \rightarrow 0, \quad \phi(\infty, \xi) \rightarrow 0. \tag{15}$$

In this study,  $\omega = b(T_w - T_\infty)$  is the temperature dependent viscous parameter,  $G_r = \frac{\xi g \beta}{a^2 x b}$  is

the modified time dependent thermal Grashof number for heat transfer parameter,  $G_s = \frac{\xi g \beta^*}{a^2 x b}$  is the modified time dependent solutal Grashof number for mass transfer parameter,  $Pr = \frac{\vartheta}{\alpha}$  is the Prandtl number,  $D_f = \frac{D_m k_f (C_w - C_\infty)}{\vartheta^* C_p C_s (T_w - T_\infty)}$  is the Dufour number,  $Sc = \frac{\vartheta^*}{D_m}$  is the Schmidt number and  $Sr = \frac{D_m K_f (T_w - T_\infty)}{\vartheta T_m (C_w - C_\infty)}$  is the Soret number. The physical quantities of interest in this problem are the skin friction coefficient, the Nusselt number and the Sherwood number which are defined as follows

$$C_f = \frac{\tau_w}{\rho u_e^2} = \frac{\vartheta}{(\alpha x)^2} \frac{\partial u}{\partial y} \Big|_{y=0}, \quad Nu = \frac{-\kappa \frac{\partial T}{\partial y} \Big|_{y=0} x}{\kappa (T_w - T_\infty)},$$

$$Sh = \frac{-D_m \frac{\partial C}{\partial y} \Big|_{y=0} x}{D_m (C_w - C_\infty)}.$$

Using the transformation variables in Eq.(10) and  $Re_x = \frac{\alpha x}{\vartheta}$  in Nath *et al.* (2002), we obtain the following dimensionless quantities

$$f''(0, \xi) = \sqrt{\xi} C_f \sqrt{Re_x}, \quad -\theta'(0, \xi) = \frac{\sqrt{\xi}}{\sqrt{x Re_x}} Nu,$$

$$-\phi'(0, \xi) = \frac{\sqrt{\xi}}{\sqrt{x Re_x}} Sh, \quad \xi > 0$$

### 3. BIVARIATE SPECTRAL RELAXATION METHOD (BSRM)

In this section the bivariate spectral relaxation method (BSRM) for solving the governing coupled non-linear system of partial differential Eq. (11) - Eq. (15) is presented following the idea in Motsa *et al.* (2015). The method starts by using Gauss-Siedel relaxation approach to rearrange and decouple Eq. (11) - Eq. (15) to form a linear sequence of partial differential equations that are later solved in succession over a number of iterations ( $r$ ). Consequently, re-arranging equations (11) - Eq. (15) and linearising in Gauss-Seidel manner gives

$$a_{0,r}(\eta, \xi) \frac{\partial^2 g_{r+1}}{\partial \eta^2} + a_{1,r}(\eta, \xi) \frac{\partial g_{r+1}}{\partial \eta} + a_{2,r}(\eta, \xi) = \xi(1 - \xi) \frac{\partial g_{r+1}}{\partial \xi}, \tag{16}$$

$$\frac{\partial f_{r+1}}{\partial \eta} = g_{r+1}, \tag{17}$$

$$\frac{\partial^2 \theta_{r+1}}{\partial \eta^2} + b_{1,r}(\eta, \xi) \frac{\partial \theta_{r+1}}{\partial \eta} + b_{2,r}(\eta, \xi) \theta_{r+1} +$$

$$b_{3,r}(\eta, \xi) = \xi(1 - \xi)Pr \frac{\partial \theta_{r+1}}{\partial \xi}, \quad (18)$$

$$\frac{\partial^2 \phi_{r+1}}{\partial \eta^2} + c_{1,r}(\eta, \xi) \frac{\partial \phi_{r+1}}{\partial \eta} + c_{2,r}(\eta, \xi) = \xi(1 - \xi)Sc \frac{\partial \phi_{r+1}}{\partial \xi}, \quad (19)$$

subject to

$$g_{r+1}(0, \xi) = 0, \quad f_{r+1}(0, \xi) = 0, \quad \theta_{r+1}(0, \xi) = 1, \quad \phi_{r+1}(0, \xi) = 1, \quad (20)$$

$$g_{r+1}(\infty, \xi) = 1, \quad \theta_{r+1}(\infty, \xi) = 0, \quad \phi_{r+1}(\infty, \xi) = 0, \quad (21)$$

where the coefficients are defined as

$$a_{0,r}(\eta, \xi) = m_1 + \omega - \omega \theta_r,$$

$$a_{1,r}(\eta, \xi) = \xi f_r + \frac{\eta}{2}(1 - \xi) - \omega \frac{\partial \theta_r}{\partial \eta},$$

$$a_{2,r}(\eta, \xi) = \xi + \omega(G_r \theta_r + G_c \phi_r) - \xi g_{r+1}^2,$$

$$b_{1,r}(\eta, \xi) = \xi Pr f_{r+1} + \frac{\eta}{2}(1 - \xi) Pr,$$

$$b_{2,r}(\eta, \xi) = \frac{B^*}{[m_1 + \omega - \theta_r \omega]}$$

$$b_{3,r}(\eta, \xi) = \frac{A^* e^{-\eta}}{[m_1 + \omega - \theta_r \omega]} + Pr D_f \frac{\partial^2 \phi_r}{\partial \eta^2},$$

$$c_{1,r}(\eta, \xi) = \xi Sc f_{r+1} + \frac{\eta}{2}(1 - \xi) Sc,$$

$$c_{2,r}(\eta, \xi) = Sc Sr \frac{\partial^2 \theta_{r+1}}{\partial \eta^2}.$$

Eq. (16) - Eq. (19) form a linear decoupled system of partial differential equations and can be solved iteratively starting from given initial approximations ( $g_0, f_0, \theta_0$  and  $\phi_0$ ). The iteration is repeated for  $r = 1, 2, \dots$ , until approximate solutions that are consistent to within a certain tolerance level are obtained. Next step is to employ the spectral collocation to discretize both space  $\eta$  and time  $\xi$  domains. The Chebyshev collocation method requires that the domain of the problem be transformed to  $[-1, 1] \times [-1, 1]$ . We therefore use simple linear transformation to

transform  $\eta \in [0, \eta_\infty]$  and  $\xi \in [0, 1]$  to  $\tau \in [-1, 1]$  and  $\zeta \in [-1, 1]$ , respectively. Here  $\eta_\infty$  is a finite value that is introduced to facilitate the application of the numerical method at infinity. The spatial and time domains are discretized using Chebyshev-Gauss-Lobatto points defined as

$$\tau_i = \cos\left(\frac{\pi i}{N_x}\right), \quad \zeta_j = \cos\left(\frac{\pi j}{N_t}\right), \quad (22)$$

$i = 0, 1, \dots, N_x; \quad j = 0, 1, \dots, N_t.$

Considering the linear decoupled system of five equations (16) - (19), each equation can be solved independently of the other equations in the system. For example, the approximate solution of  $g(\eta, \xi)$  can be obtained using bivariate Lagrange interpolation polynomial of the form

$$g(\eta, \xi) \approx \sum_{m=0}^{N_x} \sum_{j=0}^{N_t} g(\tau_m, \zeta_j) L_m(\tau) L_j(\zeta), \quad (23)$$

which interpolates  $g(\eta, \xi)$  at the collocation points defined by equation (22). We remark that, for ease of notation, we have dropped the subscripts  $r + 1$ . The functions  $L_m(\tau)$  are the well-known characteristic Lagrange cardinal polynomials

$$L_m(\tau) = \prod_{m=0, m \neq k}^{N_x} \frac{\tau - \tau_k}{\tau_m - \tau_k},$$

$$L_m(\tau_k) = \delta_{mk} = \begin{cases} 0 & \text{if } m \neq k \\ 1 & \text{if } m = k \end{cases}. \quad (24)$$

The function  $L_j(\zeta)$  is defined in a similar manner. Eq. (23) is then substituted in Eq. (16). A key step in the substitution process is the evaluation of the derivatives of  $L_m(\tau)$  and  $L_j(\zeta)$  with respect to  $\tau$  and  $\zeta$  respectively. Following Canuto *et al.* (1988), Trefethen (2000) and Motsa *et al.* (2015), we define the derivatives of  $g(\eta, \xi)$  with respect to  $\eta$  and  $\xi$  at the collocation points  $\tau_k$  and  $\zeta_i$  as follows:

$$\frac{\partial g}{\partial \eta} \Big|_{(\tau_k, \zeta_i)} = \frac{2}{\eta_\infty} \sum_{m=0}^{N_x} \sum_{j=0}^{N_t} g(\tau_m, \zeta_j) \frac{dL_m(\tau_k)}{d\tau} L_j(\zeta_i) = \mathbf{D}\mathbf{G}_i, \quad (25)$$

$$\frac{\partial^2 g}{\partial \eta^2} \Big|_{(\tau_k, \zeta_i)} = \mathbf{D}^2 \mathbf{G}_i, \quad (26)$$

$$\left. \frac{\partial g}{\partial \xi} \right|_{(\tau_k, \xi_i)} = 2 \sum_{m=0}^{N_x} \sum_{j=0}^{N_t} g(\tau_m, \xi_j) \frac{dL_j(\xi_i)}{d\xi} L_m(\tau_k) = 2 \sum_{j=0}^{N_t} d_{ij} \mathbf{G}_j, \tag{27}$$

where  $d_{i,j}$  ( $i, j = 0, 1, \dots, N_t$ ) are entries of the standard Chebyshev differentiation matrix  $d = [d_{i,j}]$  of size  $(N_t + 1) \times (N_t + 1)$  (for details, see Canuto *et al.* (1988), Trefethen (2000) and Motsa *et al.* (2015)),  $\mathbf{D} = (2/\eta_e)[D_{r,s}]$  ( $r, s = 0, 1, 2, \dots, N_x$ ) with  $[D_{r,s}]$  being an  $(N_x + 1) \times (N_x + 1)$  Chebyshev derivative matrix, and the vector  $\mathbf{G}_i$  is defined as

$$\mathbf{G}_i = [g_i(\tau_0), g_i(\tau_1), \dots, g_i(\tau_{N_x})]^T. \tag{28}$$

Accordingly, applying the collocation method with the above definitions on Eq. (16) gives

$$\mathbf{A}_i \mathbf{G}_{r+1,i} + \mathbf{a}_{2,r}(\xi_i) - 2\xi_i(1 - \xi_i) \sum_{j=0}^{N_t} d_{i,j} \mathbf{G}_{r+1,j} = 0, \tag{29}$$

$$i = 0, 1, 2, \dots, N_t,$$

subject to the boundary conditions

$$g_{r+1,i}(\tau_{N_x}) = 0, \quad g_{r+1,i}(\tau_0) = 1, \tag{30}$$

where

$$\mathbf{A}_i = \mathbf{a}_{0,r}(\xi_i) \mathbf{D}^2 + \mathbf{a}_{1,r}(\xi_i) \mathbf{D},$$

$\mathbf{a}_{m,r}(\xi_i)$  ( $m = 0, 1$ ) is the diagonal matrix of the vector  $[a_{m,r}(\tau_0), a_{m,r}(\tau_1), \dots, a_{m,r}(\tau_{N_x})]^T$  and  $\mathbf{a}_{2,r}(\xi_i) = [a_{2,r}(\tau_0), a_{2,r}(\tau_1), \dots, a_{2,r}(\tau_{N_x})]^T$ . Expanding Eq. (29) and imposing boundary conditions for  $i = 0, 1, \dots, N_t$  gives the following matrix equation:

$$\begin{bmatrix} A_{0,0} & A_{0,1} & \cdots & A_{0,N_t} \\ A_{1,0} & A_{1,1} & \cdots & A_{1,N_t} \\ \vdots & \vdots & \ddots & \vdots \\ A_{N_t,0} & A_{N_t,1} & \cdots & A_{N_t,N_t} \end{bmatrix} \begin{bmatrix} \mathbf{G}_{r+1,0} \\ \mathbf{G}_{r+1,1} \\ \vdots \\ \mathbf{G}_{r+1,N_t} \end{bmatrix} = \begin{bmatrix} \mathbf{R}_{1,0} \\ \mathbf{R}_{1,1} \\ \vdots \\ \mathbf{R}_{1,N_t} \end{bmatrix}, \tag{31}$$

where

$$A_{i,i} = \mathbf{A}_i - 2\xi_i(1 - \xi_i)d_{i,i}\mathbf{I}, \quad i = 0, 1, \dots, N_t - 1,$$

$$A_{i,j} = -2\xi_i(1 - \xi_i)d_{i,j}\mathbf{I}, \quad \text{when } i \neq j,$$

$$\mathbf{R}_{1,i} = -\mathbf{a}_{2,r}(\xi_i),$$

where  $\mathbf{I}$  is an  $(N_x + 1) \times (N_x + 1)$  identity matrix. Similarly, applying the bivariate collocation as described above on Eq. (18) and Eq. (19) gives

$$\mathbf{B}_i \Theta_{r+1,i} + \mathbf{b}_{2,r}(\xi_i) - 2\xi_i(1 - \xi_i)Pr \sum_{j=0}^{N_t} d_{i,j} \Theta_{r+1,j} = 0, \tag{32}$$

$$i = 0, 1, 2, \dots, N_t,$$

$$\mathbf{C}_i \Phi_{r+1,i} + \mathbf{c}_{2,r}(\xi_i) - 2\xi_i(1 - \xi_i)Sc \sum_{j=0}^{N_t} d_{i,j} \Phi_{r+1,j} = 0, \tag{33}$$

$$i = 0, 1, 2, \dots, N_t,$$

subject to the boundary conditions

$$\theta_{r+1,i}(\tau_{N_x}) = 0, \quad \theta_{r+1,i}(\tau_0) = 1, \quad \phi_{r+1,i}(\tau_{N_x}) = 0,$$

$$\phi_{r+1,i}(\tau_0) = 1, \tag{34}$$

where

$$\mathbf{B}_i = \mathbf{D}^2 + \mathbf{b}_{1,r}(\xi_i)\mathbf{D},$$

$$\mathbf{C}_i = \mathbf{D}^2 + \mathbf{c}_{1,r}(\xi_i)\mathbf{D},$$

$$\Theta_i = [\theta_i(\tau_0), \theta_i(\tau_1), \dots, \theta_i(\tau_{N_x})]^T,$$

$$\Phi_i = [\phi_i(\tau_0), \phi_i(\tau_1), \dots, \phi_i(\tau_{N_x})]^T,$$

$\mathbf{b}_{m,r}(\xi_i), \mathbf{c}_{m,r}(\xi_i)$  ( $m = 0, 1$ ) are the diagonal matrices of the vector  $[b_{m,r}(\tau_0), b_{m,r}(\tau_1), \dots, b_{m,r}(\tau_{N_x})]^T$  and  $[c_{m,r}(\tau_0), c_{m,r}(\tau_1), \dots, c_{m,r}(\tau_{N_x})]^T$ ,  $\mathbf{b}_{2,r} = [b_{2,r}(\tau_0), b_{2,r}(\tau_1), \dots, b_{2,r}(\tau_{N_x})]^T$  and  $\mathbf{c}_{2,r} = [c_{2,r}(\tau_0), c_{2,r}(\tau_1), \dots, c_{2,r}(\tau_{N_x})]^T$ .

Expanding Eq. (32) and Eq. (33) and imposing the boundary conditions for  $(i = 0, 1, \dots, N_t - 1)$  gives the following matrix equations:

$$\begin{bmatrix} B_{0,0} & B_{0,1} & \cdots & B_{0,N_t} \\ B_{1,0} & B_{1,1} & \cdots & B_{1,N_t} \\ \vdots & \vdots & \ddots & \vdots \\ B_{N_t,0} & B_{N_t,1} & \cdots & B_{N_t,N_t} \end{bmatrix} \begin{bmatrix} \Theta_{r+1,0} \\ \Theta_{r+1,1} \\ \vdots \\ \Theta_{r+1,N_t} \end{bmatrix} = \begin{bmatrix} \mathbf{R}_{2,0} \\ \mathbf{R}_{2,1} \\ \vdots \\ \mathbf{R}_{2,N_t} \end{bmatrix}, \tag{35}$$

$$\begin{bmatrix} C_{0,0} & C_{0,1} & \cdots & C_{0,N_t} \\ C_{1,0} & C_{1,1} & \cdots & C_{1,N_t} \\ \vdots & \vdots & \ddots & \vdots \\ C_{N_t,0} & C_{N_t,1} & \cdots & C_{N_t,N_t} \end{bmatrix} \begin{bmatrix} \Phi_{r+1,0} \\ \Phi_{r+1,1} \\ \vdots \\ \Phi_{r+1,N_t-1} \end{bmatrix} =$$

**Table 1 Comparison of  $f''(\eta = 0, \xi = 0)$  with  $P_r$  using BSRM and `bvp4c`**

	$f''(\eta = 0, \xi = 0)$ BSRM	$f''(\eta = 0)$ <code>bvp4c</code> ( $\eta_\infty = 40$ )
$P_r = 0.4$	1.07917690	1.07917690
$P_r = 0.5$	1.03517860	1.03517860
$P_r = 0.71$	0.98991357	0.98991357
$P_r = 1$	0.95924746	0.95924746

**Table 2 Comparison of  $-\theta'(\eta = 0, \xi = 0)$  with  $P_r$  using BSRM and `bvp4c`**

	$-\theta'(\eta = 0, \xi = 0)$ BSRM	$-\theta'(\eta = 0)$ <code>bvp4c</code> ( $\eta_\infty = 40$ )
$P_r = 0.4$	-0.19127669	-0.19127669
$P_r = 0.5$	-0.06753863	-0.06753863
$P_r = 0.71$	0.08927300	0.08927300
$P_r = 1$	0.23007191	0.23007191

$$\begin{bmatrix} \mathbf{R}_{3,0} \\ \mathbf{R}_{3,1} \\ \vdots \\ \mathbf{R}_{3,N_t} \end{bmatrix}, \quad (36)$$

where

$$\begin{aligned} B_{i,i} &= \mathbf{B}_i - 2Pr\xi_i(1 - \xi_i)d_{i,i}\mathbf{I}, \quad i = 0, 1, \dots, N_t, \\ B_{i,j} &= -2Pr\xi_i(1 - \xi_i)d_{i,j}\mathbf{I}, \quad \text{when } i \neq j, \\ \mathbf{R}_{2,i} &= -\mathbf{b}_{2,r}(\xi_i), \quad \mathbf{R}_{3,i} = -\mathbf{c}_{2,r}(\xi_i), \\ C_{i,i} &= \mathbf{C}_i - 2Sc\xi_i(1 - \xi_i)d_{i,i}\mathbf{I}, \quad i = 0, 1, \dots, N_t - 1, \\ C_{i,j} &= -2Sc\xi_i(1 - \xi_i)d_{i,j}\mathbf{I}, \quad \text{when } i \neq j. \end{aligned}$$

The approximate solutions for  $g(\eta, \xi)$ ,  $\theta(\eta, \xi)$  and  $\phi(\eta, \xi)$  are obtained by iteratively solving the matrix equations Eq. (31), Eq. (35) and Eq. (36), in turn, for  $r = 0, 1, 2, \dots$ . Simple exponential functions that satisfy the boundary conditions Eq. (14) and Eq. (15) can be used as initial approximations to start the iterative process at  $r = 0$ . In this work the following functions

$$\begin{aligned} f_0(\eta, \xi) &= \eta + e^{-\eta} - 1, \\ \theta_0(\eta, \xi) &= e^{-\eta}, \quad \phi_0(\eta, \xi) = e^{-\eta}. \end{aligned} \quad (37)$$

were used as initial approximations.

### 3.1 Verification of the Results

In order to verify the accuracy of the present analysis, the results of Bivariate Spectral Relaxation Method (BSRM) have been compared with that of MATLAB Package (`bvp4c`) solution for the limiting case when  $\xi = 0$ ,  $m_1 = 1$ ,  $\omega = 0.2$ ,  $G_t = G_s = 1$ ,  $A = B = 0.2$ ,  $D_f = S_r = 0.1$  and  $S_c = 0.62$  at various values of  $P_r$ .

The comparison in the above case is found to be in good agreement, as shown in Table 1 – 3. The excellent agreement is an encouragement for further study of the effects of other parameters on the fluid flow.

## 4. RESULTS AND DISCUSSION

The approximate numerical solutions of the governing systems of Eqs. (11) - (15) were

**Table 3 Comparison of  $-\phi'(\eta = 0, \xi = 0)$  with  $P_r$  using BSRM and `bvp4c`**

	$-\phi'(\eta = 0, \xi = 0)$ BSRM	$-\phi'(\eta = 0)$ <code>bvp4c</code> ( $\eta_\infty = 40$ )
$P_r = 0.4$	0.46191854	0.46191854
$P_r = 0.5$	0.45668721	0.45668721
$P_r = 0.71$	0.44969034	0.44969034
$P_r = 1$	0.44300657	0.44300657

solved using BSRM as described in the previous section. Grid independence tests revealed that  $N_x = 60$  and  $N_t = 20$  collocation points in the  $\eta$  and  $\xi$  domain, respectively, were sufficient to give accurate and consistent results. A further increase in the number of collocation points did not result in a change in the computed results. Furthermore, the minimum number of iterations required to give results that are consistent to within a tolerance level of  $10^{-5}$  were used. In all the results presented below, it was found that 30 iterations were sufficient to give consistent results. The value of  $\eta_\infty$  was set to be 10. In this section, we present the results of the numerical computations for the velocity, temperature and species concentration profiles for the various input parameters. It is very important to note that coupled dimensionless partial differential Eq. (11) - Eq. (15) can only be solved by MATLAB package (`bvp4c`) when  $\xi = 0$  and  $\xi = 1$ . In order to investigate the behavior of the fluid flow over a vertical surface, BSRM is employed. The effects of dimensionless time ( $\xi$ ) on local skin friction coefficient  $f''(\eta = 0, \xi)$ , Nusselt number that is proportional to local heat transfer rate  $-\theta'(\eta = 0, \xi)$  and Sherwood number that is proportional to local mass transfer rate  $-\phi'(\eta = 0, \xi)$  is presented in Table 4. When  $\xi = 0$ , this corresponds to initial unsteady stage. Physically, only unsteady acceleration dominates at this stage. Small magnitudes of  $f''(\eta = 0, \xi)$ ,  $-\theta'(\eta = 0, \xi)$  and  $-\phi'(\eta = 0, \xi)$  are observed when  $\xi = 0$  in 4. As  $\xi \rightarrow 0.7$ , the influence of convective acceleration terms in the dimensionless momentum equation (11), dimensionless energy equation (12) and dimensionless concentration (mass)

**Table 4** Variation of  $f''(\eta, \xi)$ ,  $-\theta'(\eta, \xi)$  and  $-\phi'(\eta, \xi)$  with dimensionless time ( $\xi$ ) using BSRM when  $m_1 = 1$ ,  $\omega = 0.2$ ,  $G_t = G_s = 1$ ,  $A = B = 0.2$ ,  $D_f = S_r = 0.1$ ,  $S_c = 0.62$  and  $P_r = 0.71$

$\xi$	$f''(\eta, \xi)$	$-\theta'(\eta, \xi)$	$-\phi'(\eta, \xi)$
0	0.989914	0.089273	0.449690
0.1	1.040608	0.092128	0.450001
0.2	1.091405	0.095787	0.450780
0.3	1.142237	0.100428	0.452115
0.4	1.193027	0.106295	0.454114
0.5	1.243676	0.113719	0.456922
0.6	1.294062	0.123160	0.460732
0.7	1.344030	0.135319	0.465812

**Table 5** Variations of  $-\phi'(0, \xi = 0)$  when  $D_f = 0.2$  and  $D_f = 1.5$  with  $S_r$  using BSRM [ $m_1 = 1$ ,  $\omega = 0.2$ ,  $G_t = G_s = 1$ ,  $A = B = 0.2$ ,  $S_c = 0.62$  and  $P_r = 0.71$ ]

$S_r$	$-\phi'(0, \xi = 0)$	
	$D_f = 0.2$	$D_f = 1.5$
0.2	0.45742873	0.49043755
0.5	0.47832951	0.59190034
0.7	0.49306220	0.69815960
0.9	0.50847774	0.86788785
1.1	0.52461694	1.18527746
$S_r$	$-\phi'(0, \xi = 0.7)$	
	$D_f = 0.2$	$D_f = 1.5$
0.2	0.47342540	0.50501860
0.5	0.49350228	0.59425037
0.7	0.50764066	0.68891866
0.9	0.52242561	0.84178897
1.1	0.53789779	1.13096612

equation (13) gradually becomes significant the fluid flow. Influence of space- and temperature-heat source as  $\xi \rightarrow 0.7$  account for the high amount of percentage increase in local heat transfer rate  $-\theta'(\eta = 0, \xi)$  which have been estimated as 51.57886%. It is observed that  $f''(\eta = 0, \xi)$  and  $-\theta'(\eta = 0, \xi)$  increases significantly with an increase in the magnitude of  $\xi$  while  $-\phi'(\eta = 0, \xi)$  increases negligibly. An increase in the magnitude of dimensionless time ( $\xi$ ) from 0 to 0.7 corresponds to 35.7724% increment in  $f''(\eta = 0, \xi)$ , 51.57886% increment in  $-\theta'(\eta = 0, \xi)$  while  $-\phi'(\eta = 0, \xi)$  increases negligibly by 3.58513%.

**4.1 Effects of Temperature Dependent Variable Viscosity Parameter  $\omega$  at Short Time and Long Time Periods**

Velocity profiles with  $\omega$  and temperature profiles with  $\omega$  when  $\xi = 0$  have been compared with when  $\xi = 0.5$  as shown in Figs. 2-5. It

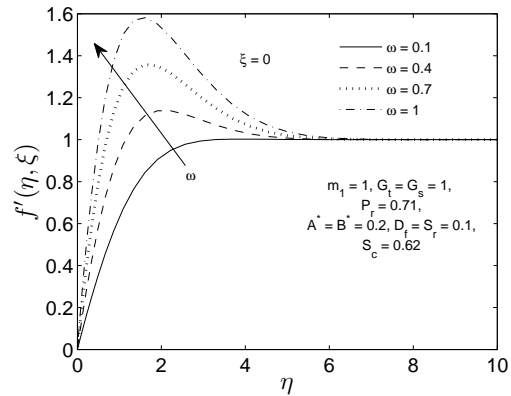


**Fig. 2.** Velocity profiles  $f'(\eta, \xi)$  for different values of temperature dependent viscous parameter ( $\omega$ ) when  $\xi = 0$  using BSRM.

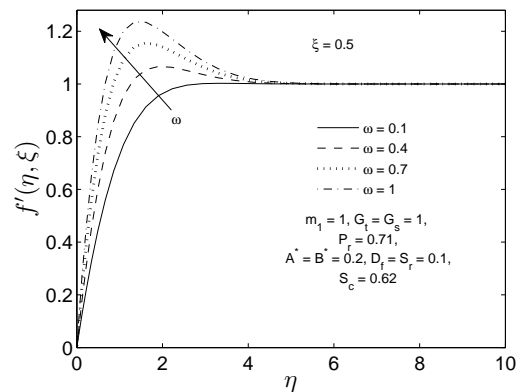


**Fig. 3.** Velocity profiles  $f'(\eta, \xi)$  for different values of temperature dependent viscous parameter ( $\omega$ ) when  $\xi = 0.5$  using BSRM.

is observed that increase in velocity function  $f'(\eta, \xi)$  due to an increase in the magnitude of temperature dependent viscous parameter is more pronounced at short time period (see Fig. 2, and Fig. 3.). Dimensionless time  $\xi$  measures the transition from short time period to long time period which corresponds to final steady stage. Firstly, it has been reported in Table 4 that  $f''(0, \xi = 0) < f''(0, \xi = 0.5)$ . Since the local skin friction when  $\xi = 0.5$  is 1.243676; physically, this indicates a negligible increase of the friction between the fluid and the heated vertical surface as  $\xi$  ranges from 0 to 0.5. Although, this kind of friction is slightly subdued by the influence of increasing parameter  $\omega$ . This accounts for the reason why velocity function  $f'(\eta, \xi = 0.5)$  still increases with  $\omega$  despite the higher magnitude of  $f''(0, \xi)$  when  $\xi = 0.5$  (i.e. unsteady acceleration and convective acceleration are present in the fluid flow owing to impulsive). Consequently, the increase in velocity

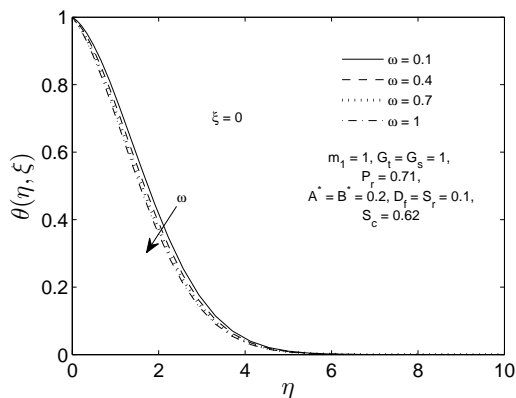


**Fig. 4. Temperature profiles  $\theta(\eta, \xi)$  for different values of temperature dependent viscous parameter ( $\omega$ ) when  $\xi = 0$  using BSRM.**

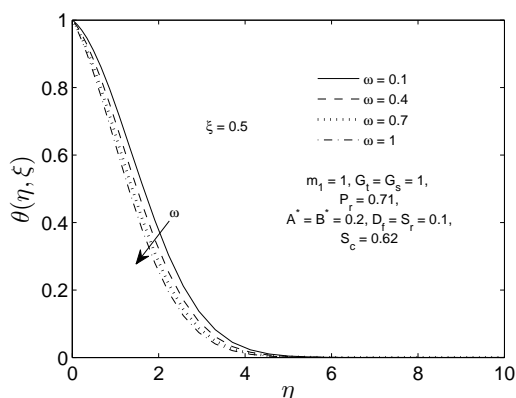


**Fig. 5. Temperature profiles  $\theta(\eta, \xi)$  for different values of temperature dependent viscous parameter ( $\omega$ ) when  $\xi = 0.5$  using BSRM.**

function with  $\omega$  at short time period  $\xi = 0$  is more enhanced than at long time period  $\xi = 1$ . It can also be deduced in Fig. 2. and Fig. 3. that an increase in the magnitude of  $\omega$  leads to a rise in the values of velocity near the vertical wall. An increase in the magnitude of  $\omega$  corresponds to an increase in the value of  $(T_w - T_\infty)$  at a constant value of  $b$ . This eventually decreases the time of interaction between neighboring molecules and the intermolecular forces between the fluid and subsequently causes a decrease in the viscosity which leads to the fluid moving faster. Furthermore, the curves show that the peak value of the velocity increases rapidly near the wall of the vertical heated plate as  $\omega$  increases and then decays as  $\eta \rightarrow \infty$ . This means that the substantial heat energy being injected from the vertical plate vanishes at larger values of  $\eta$ .

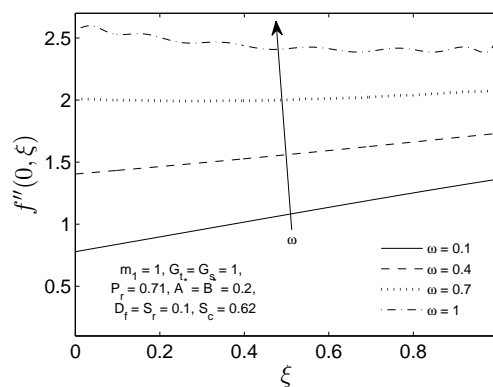


**Fig. 6. Variations of local skin friction coefficient  $f''(\eta = 0, \xi)$  with dimensionless time  $\xi$  for different values of temperature dependent viscous parameter ( $\omega$ ).**

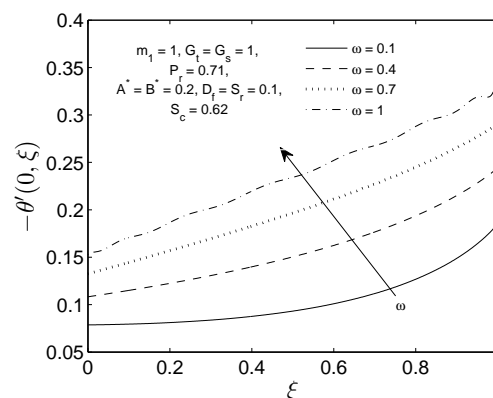


**Fig. 7. Variations of Nusselt number  $-\theta'(\eta = 0, \xi)$  with dimensionless time  $\xi$  for different values of temperature dependent viscous parameter ( $\omega$ ).**

An increase in the magnitude of  $\omega$  can be seen to reduce the temperature as shown in Fig. 4. and Fig. 5. A negligible decrease in temperature function  $\theta(\eta, \xi)$  with  $\omega$  is observed at short time period  $\xi = 0$  while a significant decrease is noticed when  $\xi = 0.5$ . At a constant value of viscosity related parameter  $b$ , as  $(T_w - T_\infty)$  increases due to the increase in the parameter  $\omega$ ; the fluid attempts to expand since it is an incompressible fluid. Thus, the fluid absorbs heat energy (temperature) available and this may account for decrease in the temperature profiles. Variations of local skin friction  $f''(0, \xi)$  which is proportional to shear stress and Nusselt number  $-\theta'(0, \xi)$  which is proportional to heat transfer rate with dimensionless time  $0 \leq \xi \leq 1$  and various values assign to  $\omega$  are presented in Fig. 6. and Fig. 7. It can be deduced from Fig. 6. that local skin friction co-

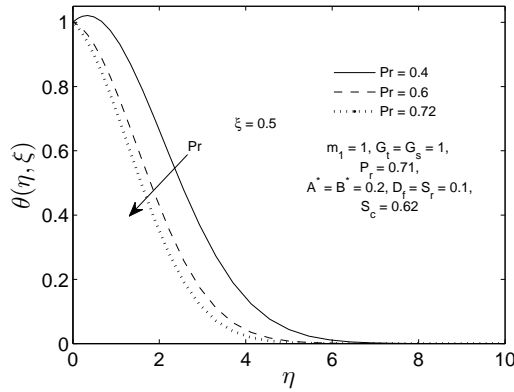


**Fig. 8. Temperature profiles  $\theta(\eta, \xi)$  for different values of Prandtl number ( $Pr$ ) when  $\xi = 0.5$  using BSRM.**

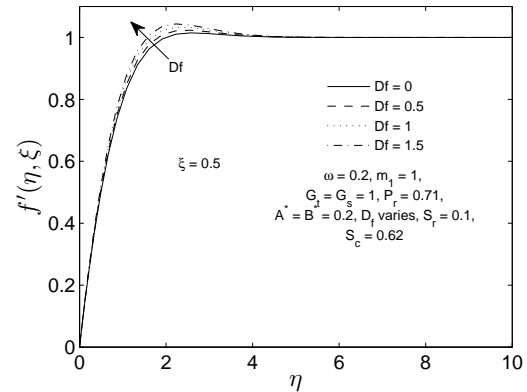


**Fig. 9. Velocity profiles  $f'(\eta, \xi)$  for different values of Dufour number ( $D_f$ ) when  $\xi = 0.5$ .**

efficient increases significantly with  $\omega$  at short time period ( $\xi = 0$ ). It is also observed that the increase in  $f''(0, \xi)$  with  $\omega$  decreases as  $\xi \rightarrow 1$ . This result implies that at any value of  $\omega < 1$ , the overall total of unsteady acceleration term in momentum, energy and concentration equations may leads to negligible effect of temperature dependent variable fluid viscosity on velocity at long time ( $\xi = 1$ ). Fig. 7. depicts that  $-\theta'(0, \xi)$  increase significantly with  $\omega$  at short time period  $\xi = 0$ . It is seen that there exist a significant increase in  $-\theta'(0, \xi)$  with  $\omega$  as  $\xi \rightarrow 1$ .

#### 4.2 Effects of Prandtl Number $P_r$ on Temperature Profiles at Long Time Period

When internal heat source parameters ( $A^* = B^*) = 0.2$ , Dufour number  $D_f = 0.1$  and Soret number  $S_r = 0.1$ , it is noticed that both conduction and convection process of heat transfer occurs as the fluid flows along a vertical heated surface (i.e.  $T_w > T_\infty$ ). The existence of the two processes of heat transfer drastically affects the temperature difference as both modes of heat transfers were competing in transferring the heat energy. It is observed in Fig. 8. that temperature distribution decreases with an increase in the magnitude of Prandtl number  $P_r$ .

#### 4.3 Effects of Dufour Number $D_f$ at Short Time and Long Time Periods

The effects of Dufour number on the velocity profiles is shown in Fig. 9. From this figure, we see that each velocity profile increases from the wall  $\eta = 0$  to a point near the wall  $\eta < 2$ . This can be traced to the effect of Blasius no-slip boundary condition. It is also observed that velocity function  $f'(\eta, \xi)$  increase negligibly with  $D_f$  within a small domain of  $\eta$  near the

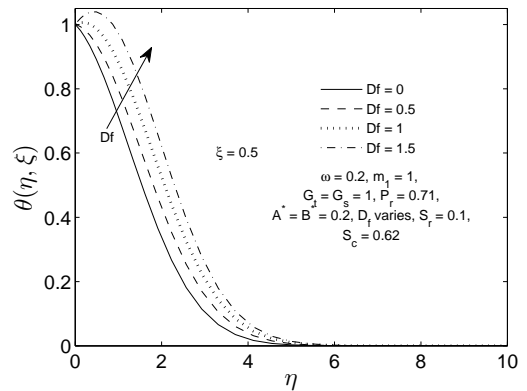


**Fig. 10. Temperature profiles  $\theta(\eta, \xi)$  for different values of Dufour number ( $D_f$ ) when  $\xi = 0.5$ .**

wall. Base on this, we may conclude that when  $Sr \ll 1$  fluid velocity rises negligibly with  $D_f$  within  $0.8 \leq \eta \leq 3.4$ .

The effects of thermo-diffusion parameter (i.e. Dufour number) on the temperature distribution is shown in Fig. 10. when  $A^* = B^* = 0.2$ ,  $Sr \ll 1$ . As  $D_f$  increases within the range  $0 \leq Df \leq 1.5$ , the temperature distribution increases significantly near the vertical heated plate  $0 \leq \eta \leq 4$ , thereafter no significant effect as  $\eta \rightarrow 10$  (fluid at free stream). The minimum distribution of temperature within the fluid domain is observed when  $D_f = 0$  (i.e. in the absence of energy flux due to composition gradient). The increasing effect  $\theta(\eta, \xi)$  with an increase in energy flux due to composition gradient is investigated at all values of  $0.01 \leq (A^*, B^*) \leq 1$ . Based on this, we may conclude that space- and temperature-dependent internal heat source contributes to this increasing effect  $\theta(\eta, \xi)$  with an increase in energy flux due to composition gradient.

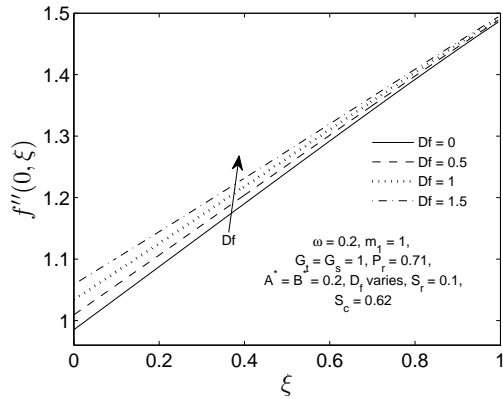


**Fig. 11.** Variations of local skin friction coefficient  $f''(\eta = 0, \xi)$  with dimensionless time  $\xi$  for different values of Dufour number ( $D_f$ ) when  $\xi = 0.5$ .

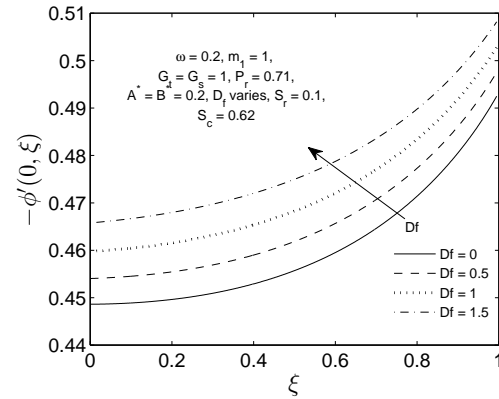


**Fig. 13.** Variations of Sherwood number  $-\phi'(\eta = 0, \xi)$  with dimensionless time  $\xi$  for different values of Dufour number ( $D_f$ ) when  $\xi = 0.5$ .

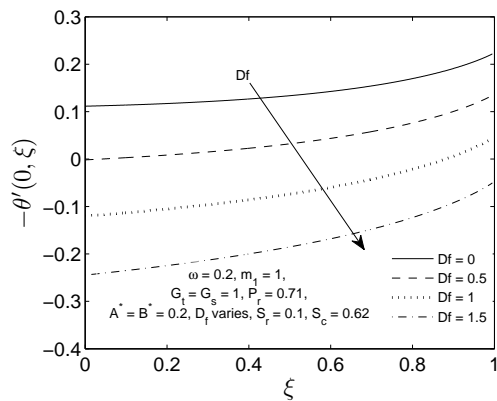


**Fig. 12.** Variations of Nusselt number  $-\theta'(\eta = 0, \xi)$  with dimensionless time  $\xi$  for different values of Dufour number ( $D_f$ ) when  $\xi = 0.5$ .

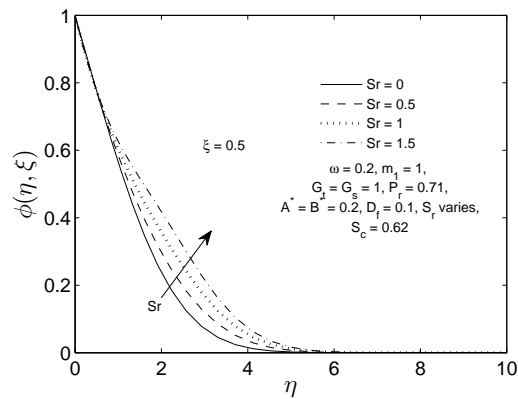


**Fig. 14.** Concentration profiles  $\phi(\eta, \xi)$  for different values of Soret number ( $S_r$ ) when  $\xi = 0.5$ .

An attempt was further made to unravel the effect of increasing Dufour parameter on physical quantities of interest (i.e. local skin friction coefficient, Nusselt number and Sherwood number) at all time  $0 \leq \xi \leq 1$  as shown in Fig. 11., Fig. 12. and Fig. 13. It is observed in both Fig. 11. and Fig. 13. that at long time period ( $\xi = 1$ ), increase in Dufour number leads to a negligible increase in local skin friction coefficient  $\sqrt{\xi}C_f\sqrt{Re_x}$  and Sherwood number  $\sqrt{\xi}/(\sqrt{xRe_x})^{-1/2}Sh$ . Also,  $D_f$  leads to a significant increase in both  $\sqrt{\xi}C_f\sqrt{Re_x}$  and  $\sqrt{\xi}/(\sqrt{xRe_x})^{-1/2}Sh$  at short time period ( $\xi = 0$ ). In addition, a significant increase in Nusselt number  $\sqrt{\xi}/(\sqrt{xRe_x})^{-1/2}Nu$  which is proportional to the rate of heat transfer with  $D_f$  is noticed at short time period as shown in Fig. 12.

#### 4.4 Effects of Soret Number $S_r$ at Short Time and Long Time Periods

Figure 14 shows the effects of Soret parameter  $S_r$  on the concentration function  $\phi(\eta, \xi)$ . We observed that when  $S_r$  increases, the concentration profiles increase significantly within fluid domain  $1 \leq \eta \leq 5$ . The negligible decrease is noticed near the vertical heated wall and concentration distributions asymptotically tend to zero within  $4 \leq \eta \leq 10$ . When the dimensionless time scale is  $1/2$ , this implies that both unsteady acceleration and convective acceleration are significant in the fluid flowing.

The negligible decrease in the concentration profiles near the wall can be traced to the low magnitude of energy flux due to concentration gradient  $1/10$  while the magnitude of mass flux due to temperature gradient increases within  $0 \leq S_r \leq 1.5$ . Variation of Sherwood

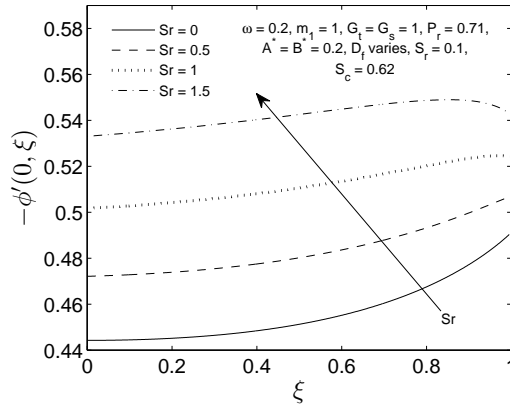


**Fig. 15. Variations of Sherwood number  $-\phi'(\eta = 0, \xi)$  with dimensionless time  $\xi$  for different values of Soret number ( $S_r$ ) when  $\xi = 0.5$ .**

number  $\sqrt{\xi}/(\sqrt{xRe_x})^{-1/2}Sh$  with  $S_r$  and  $\xi$  is presented in Fig. 15. It is observed that Soret number has significant increasing effect on  $\sqrt{\xi}/(\sqrt{xRe_x})^{-1/2}Sh$  which is proportional to local mass transfer rate at short time period ( $\xi = 0$ ). The rate at which  $-\phi'(0, \xi)$  increases with  $\xi$  in the absence of diffusion-thermo is more significant than when  $S_r = 1.5$ . The negligible increase in the magnitude of  $\sqrt{\xi}/(\sqrt{xRe_x})^{-1/2}Sh$  with  $\xi$  as shown in Fig. 15. calls for further investigation of the effect of Soret number ( $S_r$ ) on  $\sqrt{\xi}/(\sqrt{xRe_x})^{-1/2}Sh$  when magnitude of Dufour number ( $D_f$ ) is small and large. At short time period, it is shown in Fig. 16. that  $\sqrt{\xi}/(\sqrt{xRe_x})^{-1/2}Sh$  when  $D_f = 0.2$  has a linear relation with  $S_r$ , and of small quantity if compared with the case when  $\sqrt{\xi}/(\sqrt{xRe_x})^{-1/2}Sh$  varies with  $S_r$  when  $D_f = 1.5$ .

### 5. CONCLUSION

In this paper, a new spectral collocation-based method derived in terms of bivariate Lagrange interpolation polynomials have been used to solve a highly nonlinear dimensionless partial differential equation which models unsteady boundary layer flow over a vertical surface in the presence of thermal diffusion and diffusion-thermo due to impulsive and buoyancy. The newly proposed method called bivariate spectral relaxation method have been successfully used to solve a strong nonlinear coupled PDE (BVP) due to the involvement of Dufour terms in energy equation and Soret term in the species (mass) equation. The derivation of the method (BSRM) was found to be straightforward because it does not depend on any linearization expansions. In fact, the discretization of the ordinary and partial derivatives is based on sim-

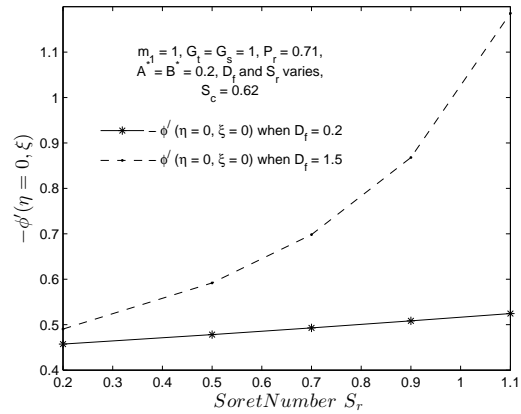


**Fig. 16. Variations of  $-\phi'(0, \xi = 0)$  when  $D_f = 0.2$  and  $D_f = 1.5$  with  $S_r$ .**

ple formulas. Since the numerical accuracy of spectral methods is very high; the number of grid points required to achieve the desired precision may be very low, thus a spectral method often requires less memory during computation. BSRM approach gives accurate solutions which are uniformly valid for all dimensionless time  $0 \leq \tau < +\infty$  in the whole region of  $0 \leq (\eta) < +\infty$  where the exact solution is not available. The effects of various physical parameters like temperature dependent variable fluid viscosity  $\omega$ , Dufour  $D_f$  and Soret number  $S_r$  were also investigated. The main findings of this investigation may be summarized as follows:

1. Increase in velocity profiles  $f'(\eta, \xi)$  with  $\omega$  when ( $\xi = 0$ ) is more pronounced than when  $\xi = 0.5$ . Maximum velocity exist at short time period of the fluid flow. Likewise, temperature profiles  $\theta(\eta, \xi)$  decreases with  $\omega$  when  $\xi = 0$  and decreases more significantly when  $\xi = 0.5$ .
2. Temperature dependent viscous parameter ( $\omega$ ) decreases temperature profile negligibly at short time period and significant decrease when  $\xi = 0.5$ . When  $(D_f, S_r) \ll 1$  and  $(G_r, G_s) = 1$   $\sqrt{\xi}/(\sqrt{xRe_x})^{-1/2}Nu$  is an increasing function of  $\omega$ . This is true at all time within the domain ( $0 \leq \xi \leq 1$ ).
3. Near the final steady stage ( $0.9 \leq \xi \leq 1$ ), Sherwood number increases when  $S_r \ll 1$  but decrease when  $S_r = 1.5$ . Within the above mentioned time interval, mass transfer rate in the absence of Soret effect is quite different from when Soret effect is present.
4. At short time period of the flow, the increasing effect of Dufour number on mass

transfer rate is more significant than on local skin friction coefficient. The increase in the magnitude of  $\sqrt{\xi}/(\sqrt{xRe_x})^{-1/2}Sh$  with  $D_f$  when  $S_f = 1.1$  is more enhanced than when  $S_f = 0.2$ . This is true at all time within the domain  $0 \leq \xi \leq 0.7$ .

5. Maximum increasing effect of  $D_f$  on  $\sqrt{\xi}/(\sqrt{xRe_x})^{-1/2}Nu$  is obtained in the absence of diffusion-thermo (Dufour effect). BSRM method can be extended to solve other types of nonlinear PDE systems with fluid mechanics applications or problems from other disciplines of science and engineering which are defined in terms of systems of non-linear PDEs.

#### ACKNOWLEDGMENTS

Authors are grateful to all the anonymous reviewers for their valuable comments and suggestions which greatly enhanced the quality and presentation of this article.

#### REFERENCES

- Alam, M., M. Ferdows, M. A. Maleque and M. Ota (2006). Dufour and soret effects on steady free convection and mass transfer flow past a semi-infinite vertical porous plate in a porous medium. *International Journal of Applied Mechanics and Engineering* 11, 535–545.
- Animasaun, I. L. (2015a). Double diffusive unsteady convective micropolar flow past a vertical porous plate moving through binary mixture using modified boussinesq approximation. *Ain Shams Engineering Journal* 7, 755–765.
- Animasaun, I. L. (2015b). Dynamics of unsteady mhd convective flow with thermophoresis of particles and variable thermo-physical properties past a vertical surface moving through binary mixture. *Open Journal of Fluid Dynamics* 5(2), 106–120.
- Batchelor, G. K. (1987). *An Introduction to Fluid Dynamics*. London: Cambridge University Press.
- Bird, R. B., W. E. Stewart and E. N. Lightfoot (2007). *Transport Phenomena (Second Edition)*. Netherlands.: John Wiley & Sons.
- Canuto, C., M. Y. Hussaini, A. Quarteroni and T. A. Zang (1988). *Spectral Methods in Fluid Dynamics*. Berlin: Springer-Verlag.
- Dennis, S. C. R. (1972). The motion of a viscous fluid past an impulsively started semi-infinite flat plate. *J. Inst. Math. and Appl.* 10, 105–117.
- El-Aziz, M. A. and A. M. Salem (2008). Effect of hall currents and chemical reaction on hydromagnetic flow of a stretching vertical surface with internal heat generation/absorption. *Applied Mathematical Modelling* 32, 1236–1254.
- Fick, A. (1855). Ueber diffusion. *Annalen der Physik und Chemie* 94, 59–86.
- Fourier, J. (1995). *The Analytical Theory of Heat*. New York, USA.: Dover Publications, Inc.
- Liao, S. (2006). An analytic solution of unsteady boundary-layer flows caused by an impulsively stretching plate. *Communications in Nonlinear Science and Numerical Simulation* 11, 326–339.
- Motsa, S. S. (2013a). A new spectral local linearization method for non-linear boundary layer flow problems. *Journal of Applied Mathematics* 2013, ID 423628.
- Motsa, S. S. (2013b). On the practical use of the spectral homotopy analysis method and local linearisation method for unsteady boundary-layer flows caused by an impulsively stretching plate. *Numerical Algorithms* 66, 865–883.
- Motsa, S. S. and I. L. Animasaun (2015). A new numerical investigation of some thermo-physical properties on unsteady mhd non-darcian flow past an impulsively started vertical surface. *Thermal Science* 19 (Suppl. 1), S249–S258.
- Motsa, S. S., Z. G. Makukula and S. Shateyi (2015). Numerical investigation of the effect of unsteadiness on three-dimensional flow of an oldroyd-b fluid. *PLoS ONE* 10(7), e0133507.
- Mukhopadhyay, S. (2009). Effects of radiation and variable fluid viscosity on flow and heat transfer along a symmetric wedge. *Journal of Applied Fluid Mechanics* 2(2), 29–34.
- Nath, G., N. Sreeshylan and R. Seshadri (2002). Unsteady mixed convection flow in the stagnation region of a heated vertical plate due to impulsive motion. *International Journal of Heat and Mass Transfer* 45, 1345–1352.
- Nazar, R., N. Amin and I. Pop (2004). Unsteady boundary layer flow due to

- stretching surface in a rotating fluid. *Mechanics Research Communications* 31, 121–128.
- Petukhov, B. and A. Poliakov (1988). *Heat Transfer in Turbulent Mixed Convection*. New York, USA.: Hemisphere Publishing Corp.
- Pop, I., N. Amin, D. Filip and R. Nazar (2004). Unsteady boundary layer flow in the region of the stagnation point on a stretching sheet. *International Journal of Engineering Science* 42, 1241–1253.
- Rashad, A. M., M. Modather and S. M. M. EL-Kabeir (2015). Heat and mass transfer by unsteady natural convection over a moving vertical plate embedded in a saturated porous medium with chemical reaction, solet and dufour effects. *Journal of Applied Fluid Mechanics* 8(3), 453–463.
- Salem, A. M. and M. A. El-Aziz (2007). Mhd-mixed convection and mass transfer from a vertical stretching sheet with diffusion of chemically reactive species and space- or temperature-dependent heat source. *Canadian Journal of Physics* 85, 359–373.
- Sandeep, N. and V. Sugunamma (2014). Radiation and inclined magnetic field effects on unsteady hydromagnetic free convection flow past an impulsively moving vertical plate in a porous medium. *Journal of Applied Fluid Mechanics* 7(2), 275–286.
- Sandeep, N., C. Sulochana and I. L. Animasaun (2016). Stagnation-point flow of a jeffrey nano fluid over a stretching surface with induced magnetic field and chemical reaction. *International Journal of Engineering Research in Africa* 20(93), 93–111.
- Sibanda, P., S. Motsa and S. Shateyi (2010). A new spectral-homotopy analysis method for solving a nonlinear second order bvp. *Commun Nonlinear Sci Numer Simulat* 15(9), 22932302.
- Stewartson, K. (1951). On the impulsive motion of a flat plate in a viscous fluid-part 1. *Quart. J. Mech. Appl. Math.* 4, 182–198.
- Stoke, G. (1901). On the effect of internal friction of fluids on the motion of pendulums, trans. cam. phil. soc. 9,8-106 (1851); mathematics and physics papers, vol. 3, p. 1. *Cambridge University Press, Cambridge* 3(1), 1–86.
- Trefethen, L. N. (2000). *Spectral Methods in MATLAB*. Philadelphia: SIAM.
- Watkins, C. B. (1975). Heat transfer in the boundary layer over an impulsively started flat plate. *J. Heat Transfer* 97, 482–484.
- Welty, J., C. Wicks, G. L. Rorrer and R. E. Wilson (1976). *Fundamentals of momentum, Heat and Mass Transfer (Fifth Edition)*. Netherlands.: John Wiley & Sons.
- Williams, J. C. and T. H. Rhyne (1980). Boundary layer development on a wedge impulsively set into motion. *SIAM Journal of Applied Mathematics* 38, 215–224.